Title

Uncertainty quantification of relative acoustic nonlinearity parameter of guided waves for damage detection in composite structures

ISBN

9781628415414

Authors

Hong, Ming
Mao, Zhu
Todd, Michael D
et al.

Publication Date

2015-03-23

DOI

10.1117/12.2084182

Peer reviewed

Uncertainty Quantification of Relative Acoustic Nonlinearity Parameter of Guided Waves for Damage Detection in Composites

Ming Hong[a,b], Zhu Mao[b], Michael D. Todd[b], Zhongqing Su*[a,c] and Xinlin Qing[d]
[a]Department of Mechanical Engineering, The Hong Kong Polytechnic University, Kowloon, Hong Kong SAR; [b]Department of Structural Engineering, University of California San Diego, 9500 Gilman Dr., La Jolla, CA USA 92093; The Hong Kong Polytechnic University Shenzhen Research Institute, Shenzhen, 518057, China; [d]Division of Aviation Health and Safety Management, Beijing Aeronautical Science and Technology Research Institute of COMAC, Beijing, 102211, China

ABSTRACT

Nonlinear guided waves have been studied extensively for the characterization of micro-damage in plate-like structures, such as early-stage fatigue and thermal degradation in metals. Meanwhile, an increasing number of studies have reported the use of nonlinear acoustic techniques for detection of impact damage, fatigue, and thermal fatigue in composite structures. Among these techniques, the (relative) acoustic nonlinearity parameter, extracted from acousto-ultrasonic waves based on second-harmonic generation, has been considered one of the most popular tools for quantifying the detection of nonlinearity in inspected structures. Considering the complex nature of nonlinearities involved in composite materials (even under healthy conditions), and operational/environmental variability and measurement noise, the calculation of the relative acoustic nonlinearity parameter (RANP) from experimental data may suffer from considerable uncertainties, which may impair the quality of damage detection. In this study, we aim to quantify the uncertainty of the magnitude of the RANP estimator in the context of impact damage identification in unidirectional carbon fiber laminates. First, the principles of nonlinear ultrasonics are revisited briefly. A general probability density function of the RANP is then obtained through numerical evaluation in a theoretical setting. Using piezoelectric wavers, continuous sine waves are generated in the sample. Steady-state responses are acquired and processed to produce histograms of the RANP estimates before and after the impact damage. These observed histograms are consistent with the predicted distributions, and examination of the distributions demonstrates the significance of uncertainty quantification when using the RANP for damage detection in composite structures.

Keywords: acoustic nonlinearity parameter, uncertainty quantification, nonlinear guided waves, statistical modeling, carbon fiber, nondestructive evaluation, structural health monitoring

1. INTRODUCTION

Composite materials have been widely used in aerospace and transportation industries. Although endowed with merits like high strength-to-weight ratio, corrosion resistance, and flexibility in design, these materials may suffer various forms of damage that are invisible or difficult to identify, primarily due to their susceptibility to foreign object impacts.[1] For example, low-velocity impacts, such as tool dropping during the manufacturing and servicing stages, may result in hidden damage inside the structure. Typical types of impact damage range from indentation and matrix micro-cracks to ply delamination and fiber breakage. Similarly, cyclic loadings, both mechanical and thermal, may also lead to matrix cracking and interlaminar damage that require early attention.

Over the last few decades, many nondestructive evaluation (NDE) methods and structural health monitoring (SHM) systems have been developed for damage detection in composite structures. Among them, acousto-ultrasonic techniques, such as guided wave testing, have been particularly popular, featuring fast and omnidirectional wave propagation and strong penetration throughout the inspected structure. However, majority of the past efforts in using guided wave testing has been focused on analyzing linear property variations caused by structural damage. As discussed in many other works,[1,2] these classical techniques may not be appropriate to apply to inhomogeneous materials, and specifically to structures whose damage size is on the same order of magnitude of the probing wavelength, which is usually the case for c o m p o s i t e

*mm.su@polyu.edu.hk; phone 852 2766-7818; fax 852 2365-4703

materials (e.g. matrix micro-cracks from impact damage).

On the other hand, nonlinear ultrasonic tools, such as nonlinear guided waves, have demonstrated their higher sensitivities to micro-defects that are common in composite materials. Aymerich and Staszewski[3] and Meo et al.[4] used a technique called nonlinear elastic wave spectroscopy (NEWS) to evaluate impact damage in composite structures. In parallel, Ciampa et al.[1] employed the second-harmonic generation mechanism of acousto-ultrasonic waves to calibrate material and damage-induced nonlinearities in a composite laminate, through finite element simulation and experiments. Pieczonka et al.[5] also studied the effectiveness of second-harmonic generation and compared it to local defect resonance (LDR) when assessing the imaging quality of impact damage. Li et al.[6] then used the relative acoustic nonlinearity parameter (RANP) extracted from second-harmonic Lamb waves to detect fatigue damage due to cyclic thermal loading in a composite panel.

In the aforementioned studies, the effectiveness of second-harmonic guided waves, particularly that of the RANP extracted therein, has been illustrated in damage detection in composites. However, inherent to the use of any signal feature for damage identification is some associated uncertainty. For instance, the RANP of Lamb waves is known to be highly sensitive to damage-induced nonlinearities in plates. Nevertheless, this sensitivity may be compromised by various types of noise: operational, environmental, measurement, and computational.[7] Moreover, the sources of nonlinearities in a composite laminate are largely multifold: even in the material's healthy state, features like voids and imperfect bonding between plies may significantly augment the noise effect. Consequently, when interpreting damage detection results, compromised RANP estimates may either produce false alarms (Type I errors) when there is no damage, or missed calls (Type II errors) when damage is indeed present. Therefore, it becomes highly necessary to understand the uncertainty involved in RANP estimates, and form a probabilistic framework under which a detection decision can be made from statistical inference.

The primary objective of this paper is to propose a statistical model to quantify the uncertainty of RANP estimates of nonlinear ultrasonic waves in composite materials, with and without the introduction of impact damage. In order to do so, the principles of nonlinear guided wave propagation are briefly revisited. Then, an analytical model is established and a general probability density function of RANP is obtained through numerical evaluation. Experimental validation is performed on a unidirectional carbon fiber plate using piezoelectric wafers. Continuous sine waves are generated as input, and steady-state signals are acquired and processed to produce RANP estimates. Observed histograms and predicted distributions of the RANP before and after the introduction of impact damage are compared. The quantified uncertainties of RANP estimates for the two material conditions may provide a level of confidence for damage state identification.

2. NONLINEAR LAMB WAVES

2.1 Relative acoustic nonlinearity parameter

Lamb waves are one type of guided waves that propagate in thin plates, characterized as in either symmetric or antisymmetric modes. Unlike bulk waves, Lamb waves are multimodal and dispersive in nature, usually with several modes propagating at the same time with different velocities.

Damage detection techniques based on nonlinear Lamb waves generally refer to scenarios where extra frequency bands, other than the fundamental (excitation) frequency, are found in the acquired Lamb wave signals. Second-harmonic generation specifically refers to the formation of second harmonics in the acquired frequency spectrum, due to nonlinear variations of material properties (i.e., small-scale damage, and typically quadratic in nature) encountered by the probing waves. Theoretically, the generation of second harmonics can be considered a first-order perturbation to the linear elastic response.[6] As a result, the solution to the nonlinear wave equation consists of two parts: the fundamental mode at the excitation frequency ω, plus the perturbed second harmonic mode at 2ω. The amplitudes of the two modes are related by the so-called acoustic nonlinearity parameter, or β, defined as

$$\beta = \frac{A_2}{A_1^2}\frac{8}{k^2 x}\gamma, \tag{1}$$

where A_1 and A_2 are the amplitudes at ω and 2ω, respectively; k is the wavenumber, x is the propagation distance, and γ is a function depending on wave parameters and medium properties,[8] which does not vary with respect to the health condition of the structure. Based on this equation, the degree of second-harmonic generation (hence the degree of nonlinearities in the inspected structure) may be determined. Normalizing β at a fixed k and x (while γ remains unchanged), Eq. (1) may be simplified into

$$RANP = \frac{A_2}{A_1^2}, \tag{2}$$

which defines the RANP, as the parameter for damage detection employed in this paper.

2.2 Cumulative second harmonic generation

Due to the multimodal and dispersive natures of Lamb waves in plate structures, their second harmonic effect is usually very weak. However, there exist certain conditions under which the fundamental wave mode is accompanied by cumulative second harmonic generation as propagation distance increases. In principle, by using the mode expansion approach, the second harmonic wave field of Lamb waves can be regarded as the superposition of a series of double-frequency wave modes.[9] Generally, the contribution from each double-frequency mode to the second harmonic wave field depends on its phase velocity in relation to that of the fundamental mode. If the fundamental mode and a particular double-frequency mode share the same phase velocity, and provided with non-zero power flux, internal resonance occurs and energy can be transferred from the fundamental mode to the second harmonic continuously as it propagates. Other double-frequency modes would decay rapidly due to material attenuation. Thus, by selecting a specific excitation frequency that enables internal resonance, cumulative second harmonics can be generated, which may ensure higher signal-to-noise ratio for damage detection purposes. Note that, most of the time, the occurrence of internal resonance also guarantees group velocity matching.[10]

The dispersion curves for a unidirectional carbon fiber/epoxy plate $[0]_8$ (thickness: 1.588 mm, tensile modulus in the fiber direction: 120.66 GPa, density: 1410 kg/m^3) are displayed in Figure 1. According to the internal resonance conditions described above, the (S1, S2) mode pair is identified as an eligible combination for cumulative second harmonic generation. The S1 mode, excited at 1.460 MHz, features a phase velocity of 9,294 m/s and a group velocity of 9,265 m/s, both of which match the corresponding values of the S2 mode at 2.920 MHz.

3. PROBABILITY MODEL FOR RANP ESTIMATION

According to Eq. (2), the nonlinearity of probing waves can be evaluated by estimating the RANP, once the amplitudes of the fundamental and the second harmonic modes are known. In practice, these two amplitudes are usually found from the

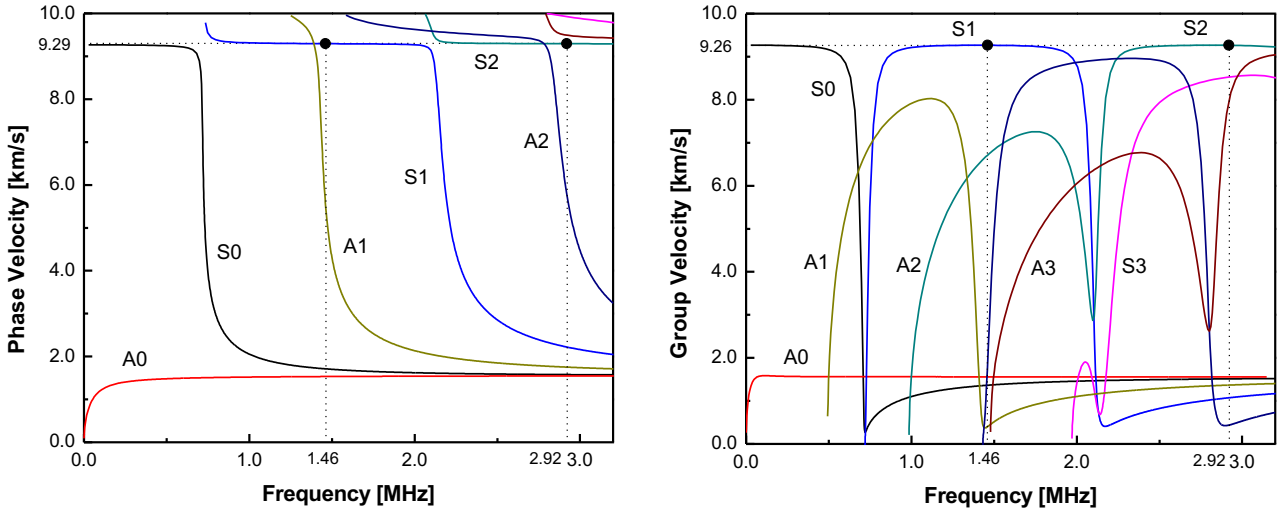

(a) (b)

Figure 1. Dispersion curves of carbon fiber/epoxy plate $[0]_8$ with 1.588 mm in thickness: (a) phase velocities; and (b) group velocities, *vs.* frequency. Mode pair (S1, S2) is marked as the candidate for cumulative second harmonic generation.

frequency spectrum of the wave signal after a fast Fourier transform (FFT). Therefore, following the definition of FFT, Eq. (2) can be rewritten as

$$RANP = \frac{\sqrt{Y_{2r}^2 + Y_{2i}^2}}{Y_{1r}^2 + Y_{1i}^2}, \tag{3}$$

where Y_{1r}, Y_{1i}, Y_{2r}, and Y_{2i} are the real and imaginary parts of the signal after transformation at ω and 2ω, respectively. For a given frequency component of the spectrum, the fundamental uncertainty in each of its real and imaginary parts is assumed to be a random variable that follows a statistically independent normal distribution. Meanwhile, these two normal distributions have the same standard deviation but different means: i.e., $Y_r \sim \boldsymbol{N}(\mu_r, \sigma^2)$, $Y_i \sim \boldsymbol{N}(\mu_i, \sigma^2)$, and $Y_r \perp Y_i$, as the Fourier transform maps the same original time series onto two orthogonal domains without discriminating the transformation gain.

Therefore, for the numerator in Eq. (3), $Y_{2r} \sim \boldsymbol{N}(\mu_{2r}, \sigma_2^2)$ and $Y_{2i} \sim \boldsymbol{N}(\mu_{2i}, \sigma_2^2)$, where σ_2 is the common standard deviation at the double frequency. Hence, the random variable $X_2 = A_2$ follows a Rice distribution, whose probability density function is given as

$$p_{X_2}(x_2) = \frac{x_2}{\sigma_2^2} \exp\left(-\frac{x_2^2 + \upsilon^2}{2\sigma_2^2}\right) I_0\left(\frac{x_2 \upsilon}{\sigma_2^2}\right), \tag{4a}$$

where $I_0(.)$ is the zero-order modified Bessel function of the first kind, and the parameter v is found by

$$\upsilon = \frac{\mu_{2r}}{\cos\left[\arctan\left(\mu_{2i} / \mu_{2r}\right)\right]} = \frac{\mu_{2i}}{\sin\left[\arctan\left(\mu_{2i} / \mu_{2r}\right)\right]}. \tag{4b}$$

Similarly, for the denominator of Eq. (3), we assume $Y_{1r} \sim \boldsymbol{N}(\mu_{1r}, \sigma_1^2)$ and $Y_{1r} \sim \boldsymbol{N}(\mu_{1r}, \sigma_1^2)$, where σ_1 is their common standard deviation at the fundamental frequency. To obtain its distribution, the denominator can be transformed as

$$A_1^2 = \sigma_1^2 \frac{A_1^2}{\sigma_1^2} = \sigma_1^2 \left[\left(\frac{Y_{1r}}{\sigma_1}\right)^2 + \left(\frac{Y_{1i}}{\sigma_1}\right)^2\right], \tag{5}$$

where the sum in the square bracket, denoted as X_1, follows a noncentral chi-square distribution, whose probability density function is given by

$$p_{X_1}(x_1) = \frac{1}{2} \exp\left(-\frac{x_1 + \lambda}{2}\right)\left(\frac{x_1}{\lambda}\right)^{k/4-1/2} I_{k/2-1}\left(\sqrt{\lambda x_1}\right). \tag{6a}$$

Since the degrees of freedom $k = 2$ in this case, Eq. (6a) retreats to

$$p_{X_1}(x_1) = \frac{1}{2} \exp\left(-\frac{x_1 + \lambda}{2}\right) I_0\left(\sqrt{\lambda x_1}\right), \tag{6b}$$

where λ is the noncentrality parameter calculated as

$$\lambda = \left(\frac{\mu_{1r}}{\sigma_1}\right)^2 + \left(\frac{\mu_{1i}}{\sigma_1}\right)^2. \tag{6c}$$

Since theoretically we have assumed the standard deviation is the same for both the real and imaginary parts, we may skip the transformation in Eq. (5) and arrive directly at Eq. (6b) as the probability density function for the variable A_1^2, using a non-normalized noncentrality parameter. However, the condition of $\sigma_{1r} = \sigma_{1i} = \sigma_1$ may not hold precisely in the experiment; thus, Eq. (5) can be retained as a way to rescale the distribution for A_1^2 by multiplying X_1 by an adjusted variance. The same argument may apply to the Rice distribution for A_2 as well.

At this point, the corresponding probability density functions for both A_2 and A_1^2 are obtained. Note that A_1 is defined earlier as the amplitude of the fundamental frequency component, instead of the largest amplitude found across the spectrum. In other words, it is the magnitude of the signal at a fixed frequency in the spectrum (i.e., at the fundamental/excitation frequency). This distinction is vital, because the frequency of the largest amplitude may vary across signals, and the real and imaginary parts of this largest amplitude in each signal do not necessarily follow the normal distributions as assumed for a given frequency. Likewise, A_2 is the amplitude retrieved at exactly twice the fundamental frequency, instead of the largest amplitude found in the neighborhood of the double frequency. Now, assuming these two random variables do not depend on each other from the perspective of signal processing, the joint probability density function of $X_1 = A_1^2 / \sigma_1^2$ and $X_2 = A_2$ may be written as

$$p_{X_1,X_2}(x_1,x_2) = \frac{x_2}{2\sigma_2^2}\exp\left(-\frac{x_1+\lambda}{2} - \frac{x_2^2+\upsilon^2}{2\sigma_2^2}\right) I_0\left(\sqrt{\lambda x_1}\right) I_0\left(\frac{x_2\upsilon}{\sigma_2^2}\right). \tag{7}$$

Therefore, the distribution of the ratio $R = X_2 / X_1$ is characterized as

$$p_R(r) = \frac{d}{dr}\left[\text{Prob}\left(\frac{X_2}{X_1} < r\right)\right] = \frac{d}{dr}\left(\iint_{\frac{X_2}{X_1}<r} p_{X_1,X_2}(x_1,x_2)dx_2dx_1\right) = \frac{d}{dr}\int_0^{+\infty}\int_0^{rx_1} p_{X_1,X_2}(x_1,x_2)dx_2dx_1. \tag{8}$$

Finally, substituting Eq. (7) into Eq. (8) yields

$$p_R(r) = \int_0^{+\infty} \frac{x_1^2 r}{2\sigma_2^2}\exp\left(-\frac{x_1+\lambda}{2} - \frac{x_1^2r^2+\upsilon^2}{2\sigma_2^2}\right) I_0\left(\sqrt{x_1\lambda}\right) I_0\left(\frac{x_1\upsilon r}{\sigma_2^2}\right) dx_1, \tag{9}$$

which does not have a further known closed-form solution. Instead, once the values of parameters λ, σ_2, and υ are retrieved from experimental data, this integral can be numerically evaluated. Figure 2 below shows representative plots of the probability density function (pdf) and the cumulative density function (cdf) of the ratio R using arbitrary parametric values. The distribution of the RANP then can be obtained by scaling the horizontal and vertical axes for the pdf by an adjusted (average) σ_1^2.

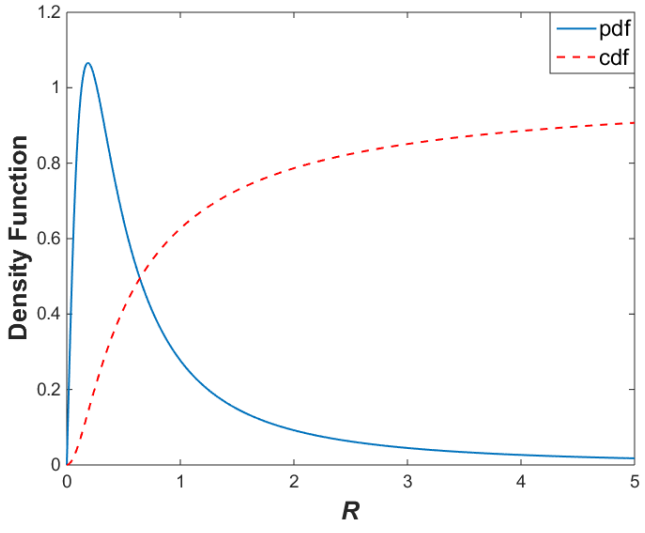

Figure 2. The probability density function and cumulative density function of R, with $\lambda = 0.6$, $\sigma_2 = 1$, and $v = 0.5$.

4. EXPERIMENTAL VALIDATION

The proposed probability model for the RANP is validated through experimentation on a unidirectional carbon fiber/epoxy laminate sample (made by ACP Composites, Livermore, CA). In the healthy condition of the structure, guided wave signals are acquired repeatedly, and from each signal a RANP estimate is calculated. A histogram of the RANP estimates can be plotted and compared to the predicted distribution. Then, impact damage is introduced to the smaple, and the measurement process is repeated.

4.1 Healthy Condition

As schematically shown in Figure 3, the sample measures 304.8 mm in length, and 152.4 mm in width; other material specifications as well as its dispersion curves have already been given in Section 2.2. Two circular piezoelectric lead zirconate titanate (PZT) wafers, 10 mm in diameter and 150 mm apart from each other, are surface-mounted on the plate to configure a sensing path along the fiber direction. An excitation frequency of 1.46 MHz is selected, according to Figure 1, for cumulative second harmonic generation, where the S1 mode can be excited in the sample as our desired fundamental mode (among other modes excited simultaneously at this frequency). In order to have output signals as stationary as possible, a continuous sinusoidal input signal, rather than windowed tone bursts that is frequently adopted in guided wave testing, is generated from a Tektronix CFG280 function generator. It is anticipated that this stationary input signal would lead to a steady-state response at the sensor, as a result of the superposition of all available guided wave modes in the structure, including the second harmonic S2 mode due to nonlinearities. Note that it has been assumed both the real and imaginary parts of the output signal at any frequency line follow normal distributions with the same standard deviation. Thus, the stationarity of output signals will directly determine the quality of the probabilistic modeling.

The experiment setup is photographed in Figure 4, in which the input signal is amplified with a power amplifier (Krohn-Hite Model 7602M) to 30 $V_{p\text{-}p}$ before going into one of the PZT wafers chosen as the actuator. Output signals are acquired at the other PZT wafer using a National Instruments® PXI platform at a sampling rate of 25 MHz. Note that wave excitation and acquisition are performed separately by the function generator and the PXI, and the input signal is channeled to another oscilloscope for reading. This way, we may avoid persistent crosstalk in the output signal. 500 acquisitions, each with a length of 16,384 points, are performed at random intervals, where uncertainties concerned may primarily come from measurement and computation. After FFT for each of the 500 signals, their frequency-domain statistics of interest are calculated and tabulated in Table 1.

It can be seen from Table 1 that, at both frequencies, the standard deviations of the real and imaginary part are relatively close to one another with four significant figures, which is consistent with our assumption of same standard deviation. Consequently, this enables a more accurate scaling from X_1, the normalized squared amplitude at the fundamental frequency, to A_1^2 using Eq. (5), using an average standard deviation such as σ_1 listed in Table 1.

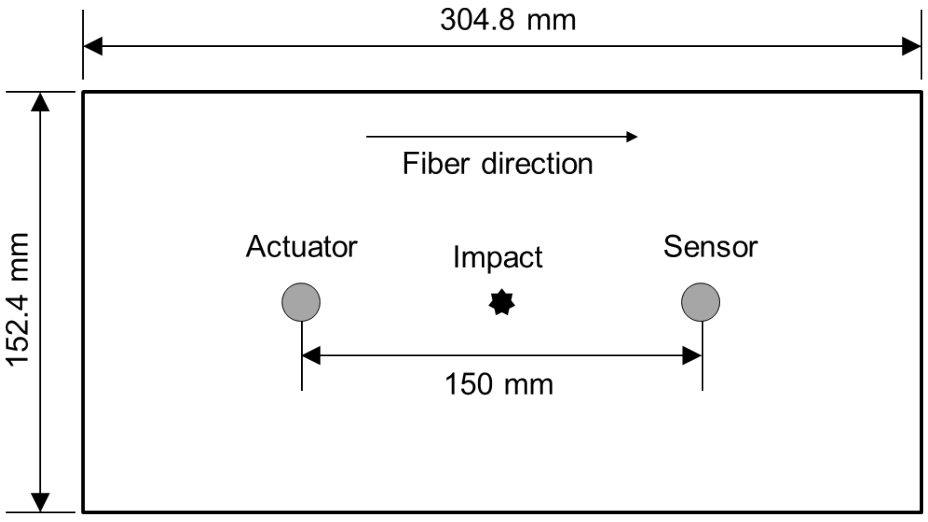

Figure 3. Schematic diagram of the carbon fiber/epoxy specimen. The impact site is near the middle of the sensing path.

Table 1. Signal statistics after FFT of 500 acquisitions.

FFT Frequency	**Real Part Mean** μ_{1r}	**Imag. Part Mean** μ_{1i}	**Real Part Std. Dev.** σ_{1r}	**Imag. Part Std. Dev.** σ_{1i}	**Average Std. Dev.** σ_1	λ
1.461 MHz	0.0080	-9.953×10^{-4}	0.3894	0.3903	0.3898	4.297×10^{-4}
FFT Frequency	**Real Part Mean** μ_{2r}	**Imag. Part Mean** μ_{2i}	**Real Part Std. Dev.** σ_{2r}	**Imag. Part Std. Dev.** σ_{2i}	**Average Std. Dev.** σ_2	ν
2.922 MHz	4.598×10^{-5}	-1.052×10^{-4}	9.048×10^{-4}	9.323×10^{-4}	9.185×10^{-4}	1.148×10^{-4}

Figure 5 shows the normalized histogram of RANP estimates from the 500 signals acquired in the healthy condition, superimposed with the predicted distribution defined by Eq. (9) using parameter values retrieved from the experiment (Table 1). As can be seen here, the histogram matches quite well with the prediction, which also validates the assumptions being made in deriving the distribution function. It is noteworthy that the predicted probability density function has an infinitely long tail extending to infinity, and in theory it does not have a well-defined order statistics. In contrast, the maximum RANP estimate obtained in the experiment is only 0.059. It is also important to point out that the predicted RANP distribution is derived purely from a signal processing perspective; thus, it is not restricted to the use for composite materials.

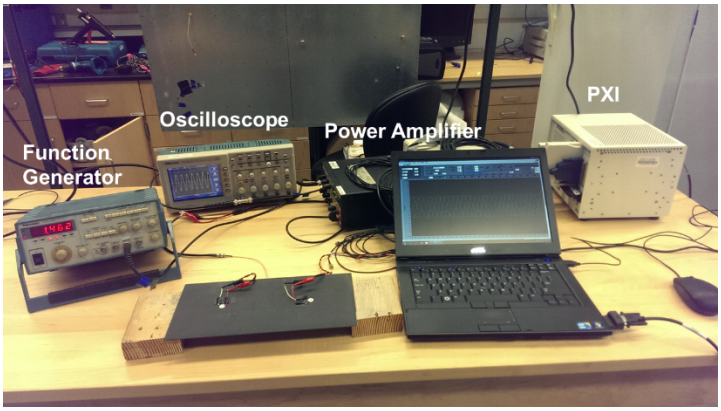

Figure 4. Experiment arrangement for testing on the composite specimen.

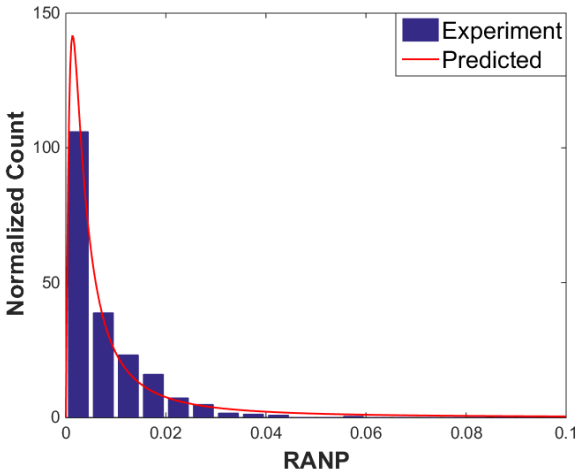

Figure 5. Histogram of RANP estimates from experiment in healthy condition *vs.* predicted distribution from Eq. (9).

4.2 Damaged Condition

A drop-weight impact test is performed with a 0.3-kg impactor, in order to introduce damage to the composite sample. It attempts to create internal damage to the material without significantly affecting the bonding conditions between the PZT wafers and the sample, which may otherwise alter the signal statistics to a great extent and reduce the repeatability of the experiment. By controlling the drop height of the impactor, the resulted impact energy is estimated to be 1.46 J. This level of energy may induce matrix cracking and minor delamination in carbon fiber laminates.[3] After the testing, the sample is re-instrumented as described in Section 4.1, leaving all the measurement settings unchanged.

Another set of 500 signals is acquired and processed with exactly the same algorithm. Figure 6 shows both the histograms and predicted distributions before and after the impact damage. To facilitate comparison, the two histograms are plotted with the same bins. It can be seen that the histogram in the damaged case has a fatter tail, extending much further to the right than the healthy one. This represents a greater probability of having a bigger RANP estimate relative to the healthy condition, which is intuitively consistent with the theory that increased nonlinearities (due to damage) will lead to an increased RANP estimate. Similarly, the two predicted distributions (blue dash-dotted line for the healthy and red dashed line for the damaged) also capture the above distinction.

While the predicted distribution does not have a well-defined expectation value as mentioned earlier, the sample mean of RANP values from the healthy data is found to be 7.55×10^{-3}, in comparison to 3.27×10^{-2} for the damaged case. With a 333% difference between the means, still, it can be observed that the separation between the two distributions or histograms is not big enough to rely on a single RANP estimate to make the judgment. Especially for RANP values less than 0.02, there is a considerable overlap between the two distributions/histograms. In other words, given the data and the plots, we do not possess enough prior knowledge of the RANP, against which a clear-cut damage identification decision can be made. Plausibly, this conclusion is not unusual for many damage detection situations, where the change in our chosen damage parameter is not significant enough to infer the true presence or absence of structural damage. Consequently, uncertainty quantification of a damage parameter becomes an indispensable tool for us to better understand what an estimate could mean, which may provide a probabilistic framework, or a quantified level of confidence, for making our next damage identification decision.

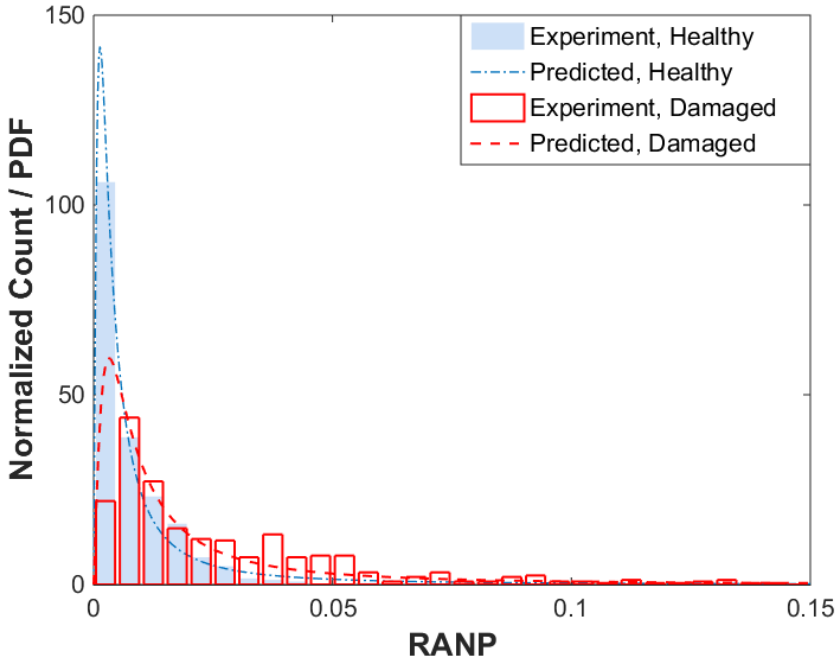

Figure 6. Histograms of RANP estimates and predicted distributions under healthy and impact damaged conditions.

5. CONCLUSIONS

In this study, the uncertainty of the relative acoustic nonlinearity parameter, a.k.a. RANP, of nonlinear guided waves is quantified for damage detection purposes. Under certain assumptions on the distributions of frequency-domain signals, a general probability density function for RANP estimates is derived. This distribution can be numerically evaluated once signal statistics from experiments are obtained. The predicted distribution is then applied to guided wave testing on unidirectional carbon fiber samples. Piezoelectric wafers are used for wave excitation and acquisition. A continuous sinusoidal signal at a chosen frequency is applied for wave excitation, enabling cumulative second harmonic generation in the material. Steady-state response is achieved and processed to extract necessary signal features. The histogram of the RANP estimates obtained matches well with the predicted distribution. Impact damage is then introduced to the sample, and the newly obtained RANP distribution exhibits a fatter tail to the right, showing a greater probability of having a larger RANP estimate relative to the healthy condition. This finding confirms the increased nonlinearities in the composite sample due to impact damage. Yet, it is found that the separation between the two distributions (before and after damage) is not significant enough to enable a confident decision making process based on individual RANP estimates. Thus, uncertainty quantification of RANP estimates in our model may serve as a probabilistic framework for making the next damage identification decision.

ACKNOWLEDGMENTS

This project is jointly supported by the Hong Kong Research Grants Council RGC via General Research Funds (No. 523313 and No. 15214414), National Natural Science Foundation of China (Grant No. 51375414), the research grant (UD130058JD) of the Agency for Defense Development of the Korean government and the Leading Foreign Research Institute Recruitment Program through the National Research Foundation of Korea funded by the Ministry of Science, ICT and Future Planning (2011-0030065). The first author would also like to acknowledge the support from Fulbright-RGC Hong Kong Research Scholar Award.

REFERENCES

[1] Ciampa, F., Onder, E., Barbieri, E. and Meo, M., "Detection and modelling of nonlinear elastic response in damaged composite structures," J. Nondestruct. Eval. 33, 515–521 (2014).

[2] Su, Z., Zhou C., Hong, M., Cheng, L., Wang Q. and Qing, X., "Acousto-ultrasonics-based fatigue damage characterization: Linear versus nonlinear signal features," Mech. Syst. Signal Proc. 45, 225–239 (2014).

[3] Aymerich, F. and Staszewski, W. J., "Impact damage detection in composite laminates using nonlinear acoustics," Compos. Part A 41, 1084–1092 (2010).

[4] Meo M., Polimeno U. and Zumpano, G., "Detecting damage in composite material using nonlinear elastic wave spectroscopy," Appl. Compos. Mater. 15, 115–126 (2008).

[5] Pieczonka, L., Klepka, A., Staszewski, W. J. and Uhl, T., "Nonlinear acoustic imaging of structural damages in laminated composites," Proc. 7th EWSHM, 1670–1675 (2014).

[6] Li, W., Cho, Y. and Achenbach, J. D., "Detection of thermal fatigue in composites by second harmonic Lamb waves," Smart Mater. Struct. 21, 085019 (2012).

[7] Mao, Z. and Todd, M., "A model for quantifying uncertainty in the estimation of noise-contaminated measurements of transmissibility," Mech. Syst. Signal Proc. 28, 470–481 (2012).

[8] Xiang, Y., Deng, M., Xuan, F.-Z. and Liu, C.-J., "Experimental study of thermal degradation in ferritic Cr-Ni alloy steel plates using nonlinear Lamb waves," NDT E. Int. 44, 768–774 (2011).

[9] Deng, M. and Pei, J., "Assessment of accumulated fatigue damage in solid plates using nonlinear Lamb wave approach," Appl. Phys. Lett. 90, 121902 (2007).

[10] Matsuda, N. and Biwa, S., "Phase and group velocity matching for cumulative harmonic generation in Lamb waves," J. Appl. Phys. 109, 094903 (2011).